International Journal of Mechanical Sciences 52 (2010) 1419–1436

Contents lists available at ScienceDirect

International Journal of Mechanical Sciences

journal homepage: www.elsevier.com/locate/ijmecsci

# Identification of the nonlinear excitation force acting on a bowed string using the dynamical responses at remote locations

Vincent Debut [a,*], X. Delaune [b], J. Antunes [a]

[a] Instituto Tecnológico e Nuclear, Applied Dynamics Laboratory, ITN/ADL, Estrada Nacional 10, 2686 Sacavem Codex, Portugal
[b] Commissariat à l'Energie Atomique, Laboratoire d'Etudes de Dynamique, CEA/DEN/DM2S/SEMT, F-01101 Gif-sur-Yvette, France

ARTICLE INFO

*Article history:*
Received 9 November 2009
Received in revised form
16 March 2010
Accepted 17 March 2010
Available online 20 March 2010

*Keywords:*
Inverse problems
Modal technique
Regularization
Optimization
Friction force
Bowed string

ABSTRACT

For achieving realistic numerical simulations of bowed string instruments, based on physical modeling, a good understanding of the actual friction interaction phenomena is of great importance. Most work published in the field including our own has assumed that bow/string frictional forces behave according to the classical Coulomb stick–slip model, with an empirical velocity-dependent sliding friction coefficient. Indeed, the basic self-excited string motions (such as the Helmholtz regime) are well captured using such friction model. However, recent work has shown that the tribological behavior of the bow/string rosin interface is rather complex, therefore the basic velocity-dependent Coulomb model may be an over-simplistic representation of the friction force. More specifically, it was suggested that a more accurate model of the interaction force can be achieved by coupling the system dynamical equations with a thermal model which encapsulates the complex interface phenomena. In spite of the interesting work performed by Askenfelt [32], a direct measurement of the actual dynamical friction forces without disturbing the string motion is quite difficult. Therefore, in this work we develop a modal-based identification technique making use of inverse methods and optimization techniques, which enables the identification of the interface force, as well as the string self-excited motion, from the dynamical reactions measured at the string end supports. The method gives convincing results using simulated data originated from nonlinear computations of a bowed string. Furthermore, in cases where the force identifications are very sensitive to errors in the transfer function modal parameters, we suggest a method to improve the modal frequencies used for the identifications. Preliminary experimental results obtained using a basic bowing device, by which the string is excited with the stick of the bow, are then presented. Our identifications, from the two dynamical string reactions, are consistent as attested by the comparison of the two available versions of the string dynamical motion and of the friction force. Furthermore, the method seems adequate to investigate the interface force for the bowed string.



## 1. Introduction

An important aspect of friction-related problems deals with the development of accurate models to simulate, as precisely as possible, the friction force acting on a bowed system and its resulting motion. Due to the complex nature of this interaction, which is highly nonlinear, several models have emerged—mostly of empirical nature—with different assumptions depending on the problem to address. Particularly, for the case of a bowed string, a classical Coulomb model—in which the friction force is a function of the sliding velocity—represents a reasonable approximation to typical behavior [1–4]. Recently, Smith and Woodhouse [5,6] measured the friction and relative sliding speed between a rosined rod and a vibrating cantilever system. They argued that the friction force cannot be expressed by the classical Coulomb model and suggested that such model is an over-simplistic representation of the stick–slip vibration in the bowed string. They proposed a rather complex model involving the temperature at the contact point and claimed that it is more appropriate for simulating the bowed string dynamics.

Experimentally, the bow-string interface force cannot be easily measured directly. To overcome this difficulty, Schumacher [7] presented a method for reconstructing the force at the bowing point using the two forces signals measured at the string's terminations. The reconstruction is accomplished by combining the force signals with the actual reflection and transmission functions which describe the wave propagation along the string. As a step forward this first attempt, two versions of the reconstruction method have also been then proposed by Woodhouse et al. [8]. The first method operates in the

* Corresponding author.
*E-mail address:* vincentdebut@itn.pt (V. Debut).

0020-7403/$ - see front matter © 2010 Elsevier Ltd. All rights reserved.
doi:10.1016/j.ijmecsci.2010.03.010

time-domain and is relatively straightforward for non-dissipative systems. However, its application on a real violin body, where dissipation exists at the extremities or through the presence of a finger on the violin fingerboard, might be delicate because the deconvolution of a frequency-dependent effect is likely to be difficult in practice. The second method, also based on a wave-propagation formulation, works in the frequency domain and could allow for dissipation. When both methods are applicable, the two approaches work well and give consistent results [8].

Recently, the present authors have extended their previous work on remote identification using wave-propagation techniques [9–11]. We presented a modal approach for extracting—from remote vibratory measurements—the vibro-impact forces, as well as vibratory responses at the support location, of gap-supported tubes under flow turbulence excitation [12]. Based on realistic simulations, we tested and assessed the accuracy of the approach. The technique performs well on simulated data, and identifications remain satisfactory even under difficult conditions, when noisy signals and less-than-exact modal parameters are considered.

In the present paper, we address the inverse problem of identifying the friction force, as well as the string dynamics, at the contact point of a bowed string from the end support reactions. A modal-based formulation is employed and the identification procedure involves regularization and optimization techniques. First, we assess the accuracy of the method with simulated data stemming from nonlinear computations of a bowed string following our preliminary work [13], and second, we apply the technique to measured signals obtained from an experimental system considering a violin string bowed by the wood stick of a bow.

In contrast to the wave-propagation approach, the modal approach asks for a large number of parameters to describe the system dynamics, which is certainly a disadvantage. However, as discussed in [8–11], the implementation of wave-propagation techniques could be delicate when boundary conditions are not perfectly known or when dissipation occurs at the end supports. In the modal approach, these effects are automatically encapsulated in the modal parameters. This fact significantly favors identification techniques based on modal formulation. However, similarly to any identification technique, our method also presents some delicate issues.

To overcome the ill-conditioning of the inverse problem and reduce its sensitivity to noise, the regularization of the transfer operator is achieved through a frequency domain procedure. The choice of an appropriate regularization parameter is based on the L-curve criterion and performed using the minimal product method [14].

As a significant feature, the problem of dealing with the imperfect knowledge of the modal parameters employed to build the system transfer function is addressed. Optimization techniques are used with the aim of obtaining from an initial set of the modal parameters a better estimate suitable for the inversion. It is shown that when realistic errors are introduced in the modal frequencies, the optimization procedure improves significantly the identifications. The method gives good results with simulated signals and its application to real data indicates that the proposed method is adequate to investigate the bowed string dynamics. Our results may ultimately give insights in the complex frictional force interactions.

## 2. Time-domain computations of the nonlinear dynamics

Time-domain simulations of a bowed string were performed to generate the reference signals needed for assessing the accuracy of the identification method. The computational approach used here has already proved its efficiency in previous works of the authors concerning bowed musical instruments [15–18]. The general approach is described in detail in [3,18].

### 2.1. Formulation for the string dynamics

We consider an ideal string of length $L$ and cross-sectional area $S$, fixed at both ends and stretched to an axial tension $T$. As in most published work, the description of the vibrating string is done focusing on the transverse displacement $y(x,t)$ of the string described basically by the wave equation:

$$\rho S\frac{\partial^2 y}{\partial t^2}-T\frac{\partial^2 y}{\partial x^2}=f(x,t), \tag{1}$$

where $\rho$ is the density of the string and $f(x,t)$ is the externally applied excitation. As illustrated in Fig. 1, a bowed string is excited by a transverse friction force. The bow acts tangentially on the surface of the string and its stick–slip action results in a form of self-excited vibration for the string motion. We retain here the assumption of a bow which contacts the string at a single point $x_c$, and therefore assumed a localized contact force $f(x_c,t)=f_c(t)\delta(x-x_c)$.

In musical acoustics, it is now well-known that modal-based formulation provides a convenient framework to perform efficient nonlinear computations for both dispersive and non-dispersive systems [3,17,19]. Adopting a modal representation of the string assumed unconstrained at the contact location and assuming damping phenomena to be proportional, the modal discretization of Eq. (1) leads to

$$\ddot{q_n}(t)+2\omega_n\zeta_n\dot{q_n}(t)+\omega_n^2 q_n(t)=\mathcal{F}_n(t), \tag{2}$$

where $q_n(t)$ are the modal amplitudes, $\omega_n$ are the circular eigenfrequencies and $\zeta_n$ are the damping values for each mode ($n=1,2,\ldots,N$). The modal forces $\mathcal{F}_n(t)$ are the projections of the contact force $f(x_c,t)$ on the mode shapes of the string $\varphi_n(x)=\sin(n\pi x/L)$, defined as

$$\mathcal{F}_n(t)=\int_0^L f(x_c,t)\varphi_n(x)\,dx=\int_0^L f_c(t)\delta(x-x_c)\varphi_n(x)\,dx=f_c(t)\varphi_n(x_c). \tag{3}$$

The physical motion at any point of the string can be computed from the modal amplitudes $q_n(t)$ by superposition:

$$y(x,t)=\sum_{n=0}^{N} q_n(t)\varphi_n(x), \tag{4}$$

and similarly for the velocities and accelerations by successive time derivation of the modal amplitudes $q_n(t)$.

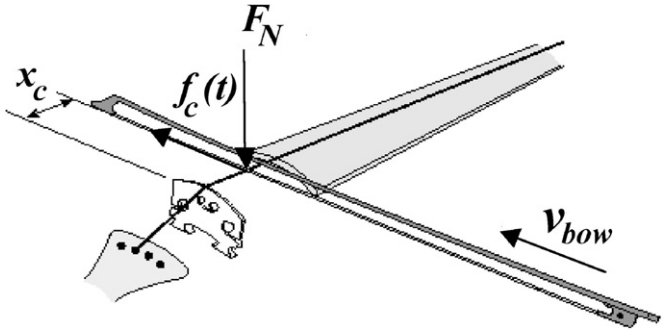


**Fig. 1.** Relevant parameters in bowed strings. $F_N$ is the normal force between the bow and the string , $v_{bow}$ is the bow velocity and $f_c(t)$ is the friction force arising between the string and the bow at location $x_c$.

### 2.2. Friction model

The friction model used in the numerical simulations is of the Coulomb type, with a velocity-dependent friction coefficient. The friction force $f_c(t)$ arising between the string and the bow at location $x_c$ of the string is given by

$$\begin{cases} f_c(t) = -\mu_d(v_c) F_N \,\mathrm{sign}(v_c) & \text{if } |v_c| > 0, \\ |f_c(t)| < \mu_S F_N & \text{if } |v_c| = 0, \end{cases} \tag{5}$$

where $F_N$ is the normal force between the bow and the string (see Fig. 1). During bow/string adherence, a (constant) static friction coefficient $\mu_S$ is used while for sliding regimes, a dynamic friction coefficient $\mu_d(v_c)$ is considered as a function of the relative bow–string velocity:

$$v_c(t) = v(x_c,t) - v_{bow}(t), \tag{6}$$

where $v_{bow}(t)$ is the bow velocity. As presented in [18], the sliding friction law model is given by

$$\mu_d(v_c) = \mu_D + (\mu_S - \mu_D) e^{-C|v_c|}, \tag{7}$$

where $0 \le \mu_D \le \mu_S$ is an asymptotic lower limit of the friction coefficient when $|\dot{y}_c(t)| \to \infty$, and $C$ controls the decay rate of the friction coefficient with the relative bow–string sliding velocity.

The implementation of the adherence model is thought by using the concept of spring/damping attachment point as presented in [3,18]. The idea is to "attach" the string to the bow at the contact point by introducing a suitable "adherence stiffness" $K_a$, and to damp-out any residual bow/string relative motion using an "adherence damping" term $C_a$. The adherence force $f_a(x_c,t)$ is then implemented as a penalty formulation, where the force is a function of the relative bow–string displacement and velocity, and computed as follows:

$$f_a(x_c,t) = -K_a y_c(t) - C_a v_c(t). \tag{8}$$

The relative displacement between the string and the bow hair is given by $y_c(t) = y(x_c,t) - y_{bow}(t)$, where $y_{bow}(t) = (t - t_a)\dot{y}_{bow}$ is the current position of the bow contact point assuming a constant bow speed, and $t_a$ is the time value when adherence is detected.

### 2.3. Numerical simulations of the nonlinear dynamical responses

For given initial conditions, the system of Eqs. (2)–(8) can be integrated using an adequate time-step integration algorithm, producing a transient and leading to a periodic motion of the string.

The bowing simulations were performed for a violin G-string pinned at both extremities, with a fundamental frequency of 196 Hz, an effective length $L = 0.33$ m and a linear density $\rho S = 3.1 \times 10^{-3}$ kg m$^{-1}$. For simplicity, the string was assumed perfect, so the natural frequencies $f_n = \omega_n/2\pi = n\,c/2L$ of the string are harmonics ($c$ is the transverse wave speed), and a constant modal damping value of $\zeta_n = 0.1\%$ was assumed for all modes. A modal basis with $N = 50$ modes was used and, for the friction law and the adherence model, the same values used in [18] are chosen ($\mu_S = 0.4$, $\mu_D = 0.2$, $C = 5$, $K_a = 10^5$ N m$^{-1}$ and a near-critical value for $C_a$). The time-domain integration of the nonlinear coupled modal equations is achieved using a constant average acceleration Newmark algorithm [20]. However, instead of implementing an iterative numerical scheme, we prefer to calculate the quantities at each time-step $t_k$ in an explicit manner from the modal forcing term at the previous time-step $t_{k-1}$, and to provide accurate results, a small time-step size of $\Delta t = 10^{-6}$ s has been used. Signals are one-second long which is long enough to reach a steady state periodic regime for these playing conditions.

Fig. 2 shows the time-histories of the displacement $y(x_c,t)$, velocity $v(x_c,t)$ and the friction force $f_c(t)$ at the bowing point $x_c = 0.03$ m when applying a normal bow force $F_N$ of 1 N and bow

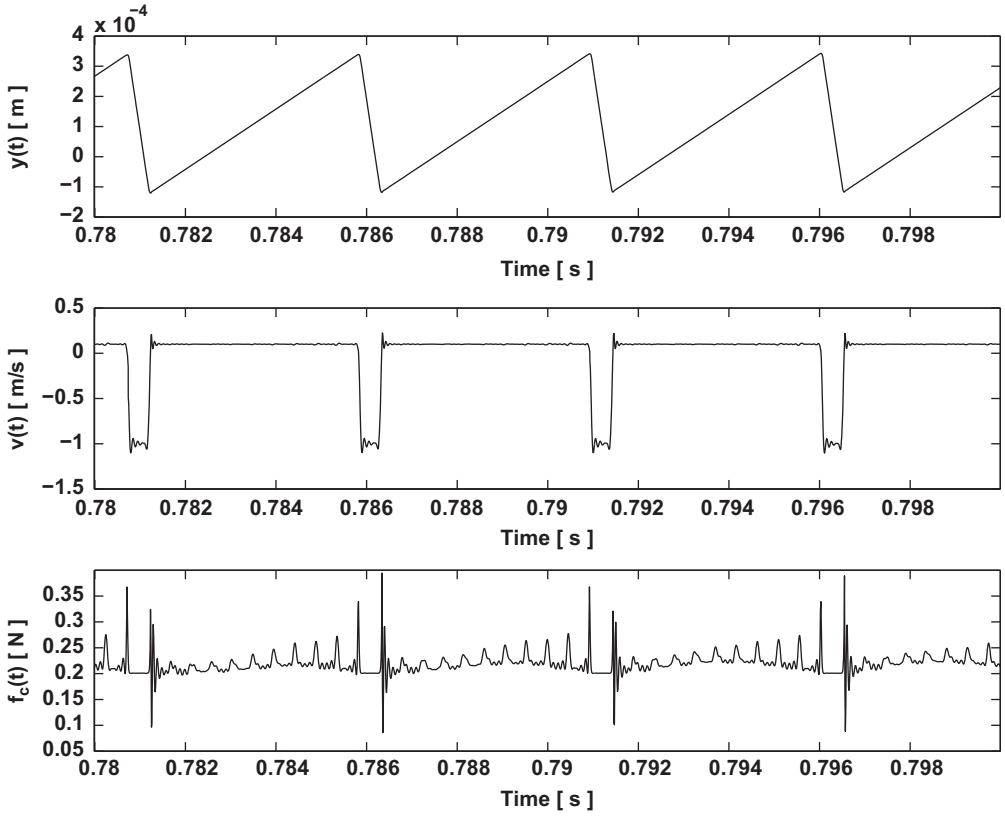


**Fig. 2.** Computed displacement, velocity and frictional force at the bow contact point $x_c = 0.03$ m, for a 0.33 m string pinned at both extremities ($F_N = 1$ N, $v_{bow} = 0.1$ m s$^{-1}$, $N = 50$ modes). Details during the steady state regime.

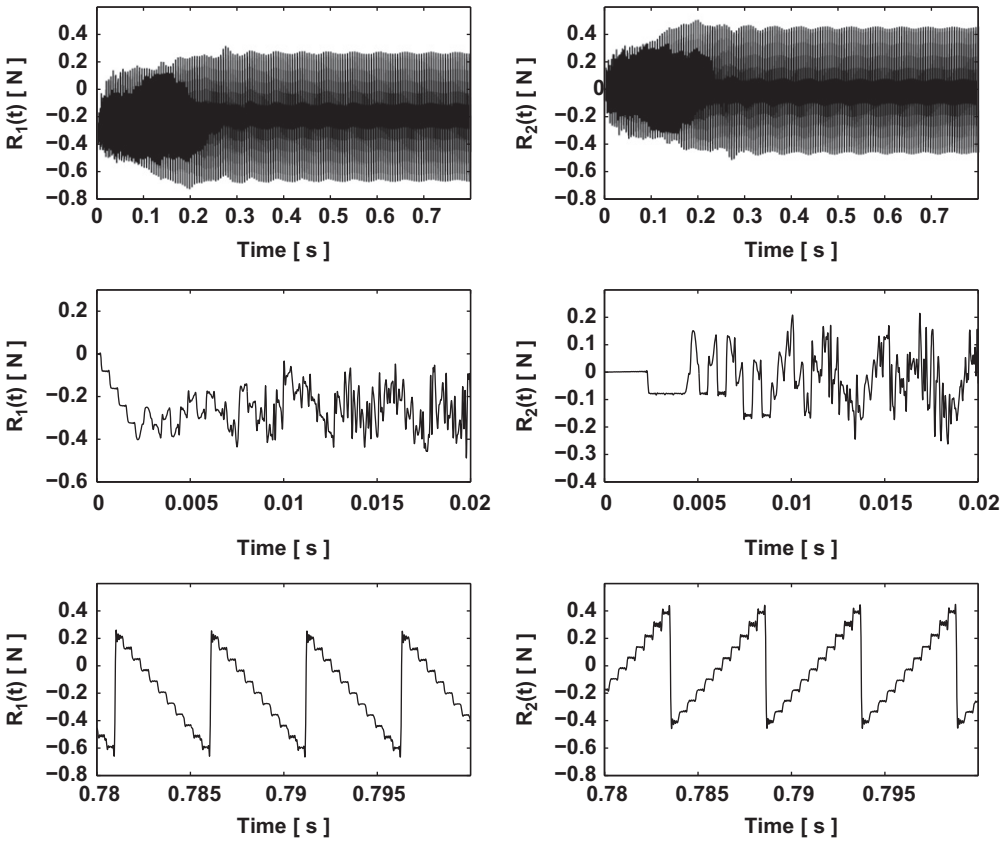


**Fig. 3.** Computed time-histories of the dynamical reactions at the two end supports (left: $x=0$; right: $x=L$) for a 0.33 m string pinned at both ends ($F_N=1$ N, $v_{bow}=0.1\,\mathrm{m\,s^{-1}}$, $x_c=0.03$ m, $N=50$ modes). Global time history trace (up) and details of the force during initial transient (middle) and steady state regime (above).

velocity $v_{bow}$ of $0.1\,\mathrm{m\,s^{-1}}$. Not unexpectedly, it shows that the string motion has developed a Helmholtz oscillating regime with the corresponding stick–slip motion. The transverse force at the two end supports are computed from the modal time response $q_n(t)$ as

$$\begin{cases} R_1(0,t) = -T\sum_{n=1}^{N} q_n(t)\left[\dfrac{\partial\varphi_n(x)}{\partial x}\right]_{x=0} = -T\sum_{n=1}^{N} q_n(t)\dfrac{n\pi}{L} \\ R_2(L,t) = T\sum_{n=1}^{N} q_n(t)\left[\dfrac{\partial\varphi_n(x)}{\partial x}\right]_{x=L} = T\sum_{n=1}^{N} q_n(t)(-1)^n\dfrac{n\pi}{L}, \end{cases} \tag{9}$$

where $T=4L^2f_1^2\rho S$ is the string tension at rest and $f_1$ is the fundamental frequency of the string. Fig. 3 shows the typical transverse force signals at the end supports of the string which will be then used as inputs for the identification procedure. Although a nonzero *dc* level appears in the support reactions in Fig. 3, our identifications will be computed from zero-mean support reaction signals, to suit the experimental conditions. As known, piezoelectric force transducers—as the ones used in our experiments (see Section 7)—are not able to measure a continuous static motion. The issue to recover the mean displacement of the string and the mean friction force is for later work. For the moment, the *dc* level will miss in both the measurements and the identifications.

## 3. Approach for source identification

As noticed earlier, no direct method of measuring the frictional force—without disturbing the string motion—can be easily achieved. So, the problem may be addressed by solving an inverse problem.

As typical for inverse problems, an important difficulty is the proper inversion of the transfer/propagation operator which describes the phenomena [12,21,22]. The ill-conditioning—physical or numerical—of the operator makes inverse problems sensitive to small perturbations, which are always present in experimental identifications. Noisy data lead to large errors in the inverse solution and regularization methods are required to reduce the noise amplification.

Other issue to be considered in system identification is the choice of the physical model. Models are typically based on well-established relationships but involve some unknown physical parameters. As a matter of fact, errors in the modeling cause further degradations of the identification procedure [9,21]. From such point of view, wave propagation approach could be attractive since only the wave speed and dissipation are required to describe the waves propagation along the string in the dispersion equation. However, the reflections and dissipation phenomena which occur at the string terminations can make its implementation delicate in practice [8,9]. In contrast to the wave approach, modal-based techniques automatically encapsulate these effects in the modal parameters. The price of this approach is that all the modal parameters, i.e. the modal mass, eigenfrequencies, damping values and modeshapes, must be determined accurately in the frequency range of interest. For example, Fig. 4 shows how bad results can be if one attempts to recover the frictional force using slightly incorrect modal frequencies in our problem. It is shown in this figure, beyond the real friction force at the contact point, the identifications of the force obtained when an uncertainty of 2% is added to the modal frequencies. To avoid such perverse effects, optimization techniques can be applied with the aim to obtain better estimates of the modal parameters before the inversion.

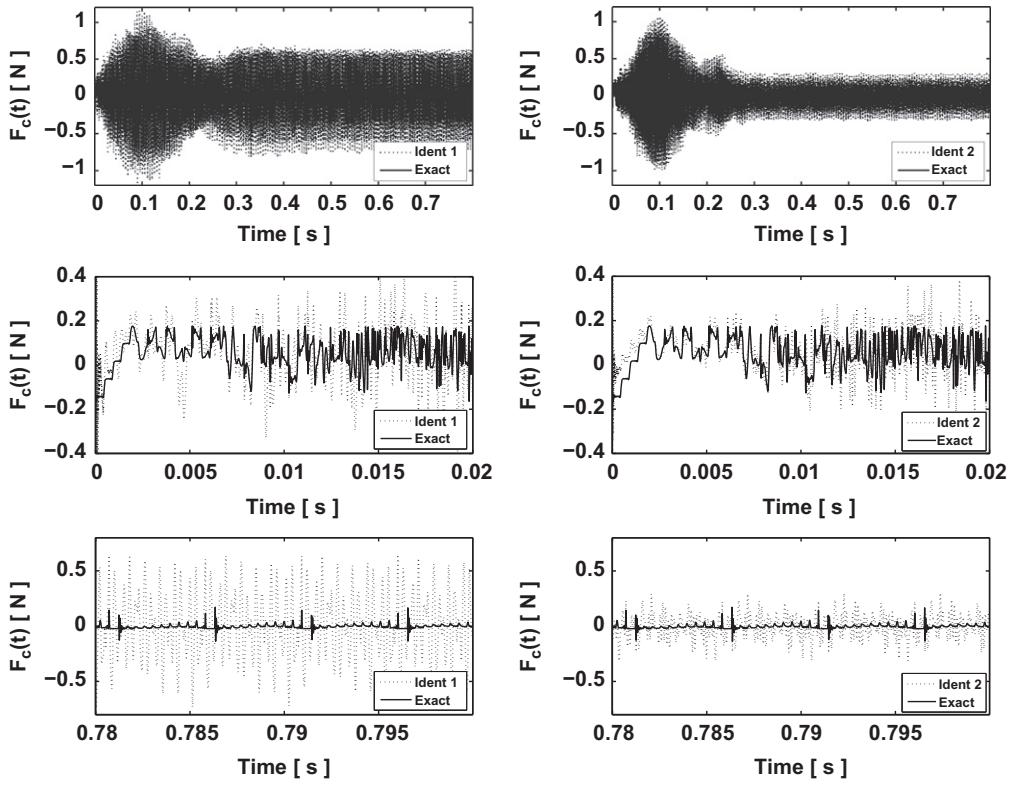


**Fig. 4.** Computed (solid) and identified (dot) time-histories of the frictional force, obtained from the support reactions at $x=0$ (left) and $x=L$ (right), when less-than-exact modal frequencies are used. Uncertainty in the modal frequencies is 2%. $N=50$ modes. Global time history trace (up) and details of the force during initial transient (middle) and steady state regime (above).

It is noteworthy that, if the nonlinear system dynamical responses are known (either from measurements or from computations), then the inverse problem of identifying the excitations (including all nonlinear interaction forces) from the available responses becomes *linear*, because the basic vibrating system may be modeled as such. In other words, once the system response is available, then even the motion-dependent forces (i.e. the friction force) can be seen as common external excitations which led to the measured string responses. Then, excitation identification becomes essentially a problem of response deconvolution, when working in the time domain, or—which is more practical—response inversion, by working in the frequency domain.

## 4. Source identification using modal formulations

Based on a linear formulation in the frequency domain, the problem of deconvolution of a contact force $F_c(x_c,\omega)$ from a reaction $R(x_r,\omega)$ measured at location $x_r$ can be summarized:

$$R(x_r,\omega)=H^{(r)}(x_c,x_r,\omega)F_c(x_c,\omega)\Longleftrightarrow F_c(x_c,\omega)=\frac{R(x_r,\omega)}{H^{(r)}(x_c,x_r,\omega)}, \tag{10}$$

where $H^{(r)}(x_c,x_r,\omega)$ is the *force-to-reaction* transfer function, built by modal superposition as

$$H^{(r)}(x_c,x_r,\omega)=\sum_{n=1}^{N}\frac{T\,\varphi_n(x_c)\varphi_n'(x_r)}{m_n[\omega_n^2-\omega^2+2i\omega\omega_n\zeta_n]}, \tag{11}$$

with $T$ the tension of the string, $i=\sqrt{-1}$ and the prime denoting spatial derivative. The displacement of the string at the contact point is computed from the estimation of the force through

$$Y(x_c,\omega)=H^{(d)}(x_c,x_c,\omega)F_c(x_c,\omega), \tag{12}$$

using the *force-to-displacement* transfer function constructed as

$$H^{(d)}(x_c,x_c,\omega)=\sum_{n=1}^{N}\frac{\varphi_n(x_c)\varphi_n(x_c)}{m_n[\omega_n^2-\omega^2+2i\omega\omega_n\zeta_n]}. \tag{13}$$

The identified velocity signal of the string at the contact point is obtained by replacing $H^{(d)}(x_c,x_c,\omega)$ in Eq. (12) by $i\omega H^{(d)}(x_c,x_c,\omega)$. Finally, the corresponding time-domain signals of the contact force $f_c(t)$, velocity $v(x_c,t)$ and displacement $y(x_c,t)$ of the string at the bowing point are computed by inverse Fourier transform. It should be noted that, even if the identification procedure involves Fourier transforms and is achieved in the frequency domain, its application to non-stationary signals is effective. Actually, the Fourier transform is not limited to periodic signals in its formulation [23]. It is the frequency resolution which plays an important role by imposing an artificial periodicity to the time signal, connected with the time window (record length). It will be shown in Section 5 that the identification of transient regimes works well in practice, provided that the record length is significantly longer than the transient duration, which usually does not constitute a problem.

Adopting a modal formulation of the system obviously leads to the important aspect of modal truncation. The choice of the number of modes $N$ to be used in the identifications (see Eqs. (11) and (13)) is problem-dependent and has to be based on the knowledge of the system. Here, to address the accuracy of our approach, a number of $N=50$ modes is used for both the identifications and the nonlinear time-domain computations. When dealing with measured signals from the experimental system, the choice of the number of modes is more critical. Ideally, all modes in the system excited frequency range should be used for identification. However, one may be interested in a somewhat narrower frequency range. On the other hand, it is useless to try identifications using higher-order modes which are

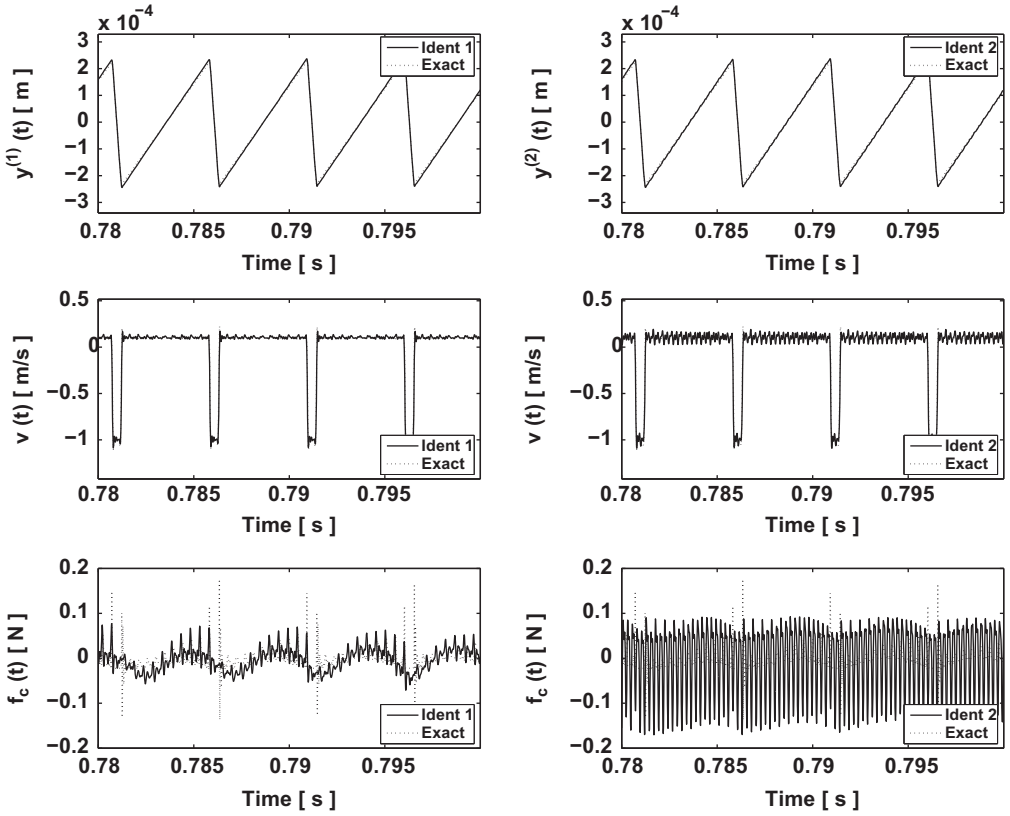


**Fig. 5.** Computed (dot) and identified (solid) time-histories of the displacement (up), velocity (middle) and frictional force (above) at the bowing contact point, obtained from the support reactions at $x=0$ (left) and $x=L$ (right), when an imperfect contact point location is used in the identification. $x_c = 0.0315$ m, $N=50$ modes. Steady state regime.

insufficiently known. These two aspects govern the truncation order which must be used in practice.

To provide a feel of the dependence of the identification approach on the contact point location $x_c$, Figs. 5 and 6 represent the identification results of the string dynamics motion and friction forces obtained by a direct inversion, using Eqs. (10)–(13)), when an error of $\pm 1.5$ mm is made in the bowing point location. As can be seen in the identified friction force, a difference in the contact point location leads to clear distinct identifications from the left and right support reactions. This dependence informs about the need of providing a correct estimate of the bowing point location for robust identifications. It also suggests that, in experimental conditions, the optimization of the contact point location can be achieved by minimizing the difference of the two waveforms of the identified friction forces. This will be done for the identifications dealing with measured signals from the experimental system.

At this stage, the computation of the inverse of the system transfer function $H$ is an important issue. Although simple in form, the computation of $1/H$ could be delicate when near-zero values of $H$ occurs. This makes inverse solution very sensitive to small changes (i.e. noisy data) and calls for the use of regularization techniques by which such sensitivity is removed.

## 5. Inverse problem regularization

To illustrate the effect of noise in the inverse solutions, Figs. 7 and 8 show the identifications of the string dynamics motion and friction forces at the bowing point, obtained from noise-free and noise-contaminated data, respectively. To simulate the noisy measurements, a Gaussian white noise of about 8% of the standard deviation of the support reaction signals has been added to the support reactions. It represents a rather difficult noisy experimental situation. The size of the modal basis is $N=50$ modes. The results in Figs. 7 and 8 show that a direct inversion (as described in Section 4) works well in a noise-free situation—recovering many details of the true results—whereas the presence of noise alters significatively the quality of the identifications. As seen in Fig. 8, if the displacement and velocity of the string are reasonable faithfull to the true result globally, the identification of the friction force is unacceptable.

To reduce the amplification of noise, the regularization of the inverse problem has to be considered. In a recent paper [12], the authors have explored two regularization techniques, a Tikhonov inspired method—perhaps the most widely used technique for regularizing ill-posed problems—and SVD filtering methods, both methods producing quite satisfying identifications. In the present paper, regularization is applied by filtering the transfer function before the inversion, similarly to the *water level regularization* technique [24]. The basic idea is to employ a modified inverse of the transfer function of the system $G^{(r)} = 1/H^{(r)}$. One notes that the deconvolution presented in Eq. (10) can be rewritten as

$$F_c(x_c,\omega) = \frac{R(x_r,\omega)}{H^{(r)}(x_c,x_r,\omega)} = R(x_r,\omega)\, G^{(r)}(x_c,x_r,\omega). \tag{14}$$

Now, the regularization of the original problem consists in replacing the operator $G^{(r)}$ by a regularized operator $G^{Reg}$, computed as follows:

$$G^{Reg}(x_c,x_r,\omega) = \begin{cases} 1/H^{(r)}(x_c,x_r,\omega) & \text{if } |H^{(r)}(x_c,x_r,\omega)| > \varepsilon, \\ 0 & \text{if } |H^{(r)}(x_c,x_r,\omega)| < \varepsilon, \end{cases} \tag{15}$$

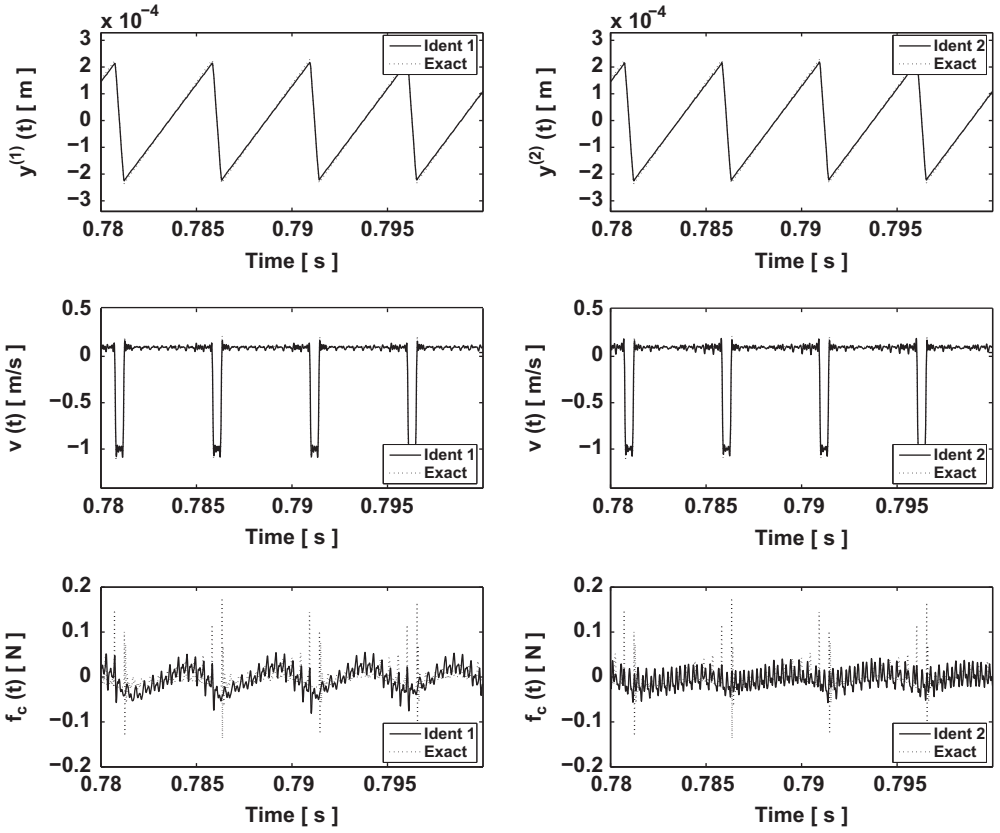


**Fig. 6.** Computed (dot) and identified (solid) time-histories of the displacement (up), velocity (middle) and frictional force (above) at the bowing contact point, obtained from the support reactions at $x=0$ (left) and $x=L$ (right), when an imperfect contact point location is used in the identification. $x_c = 0.0285$ m, $N=50$ modes. Steady state regime.

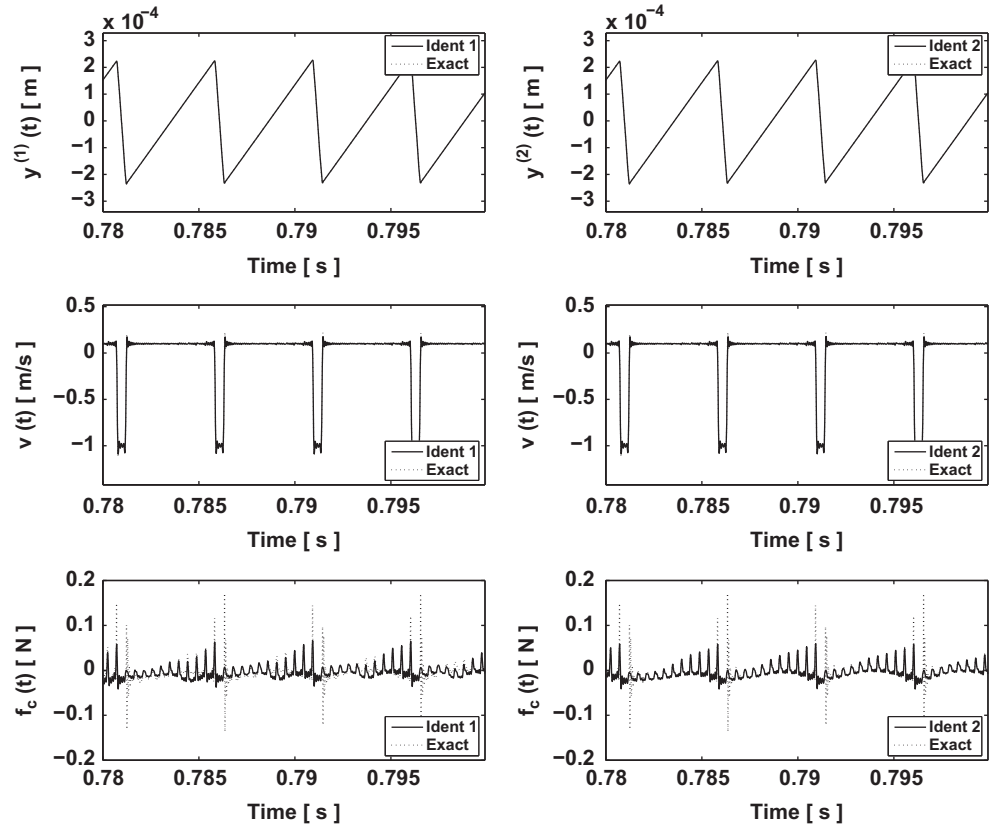


**Fig. 7.** Computed (dot) and identified (solid) time-histories of the displacement (up), velocity (middle) and frictional force (above) at the bowing contact point, obtained from the noise-free support reactions at $x=0$ (left) and $x=L$ (right). No regularization technique is used. $N=50$ modes. Steady state regime.

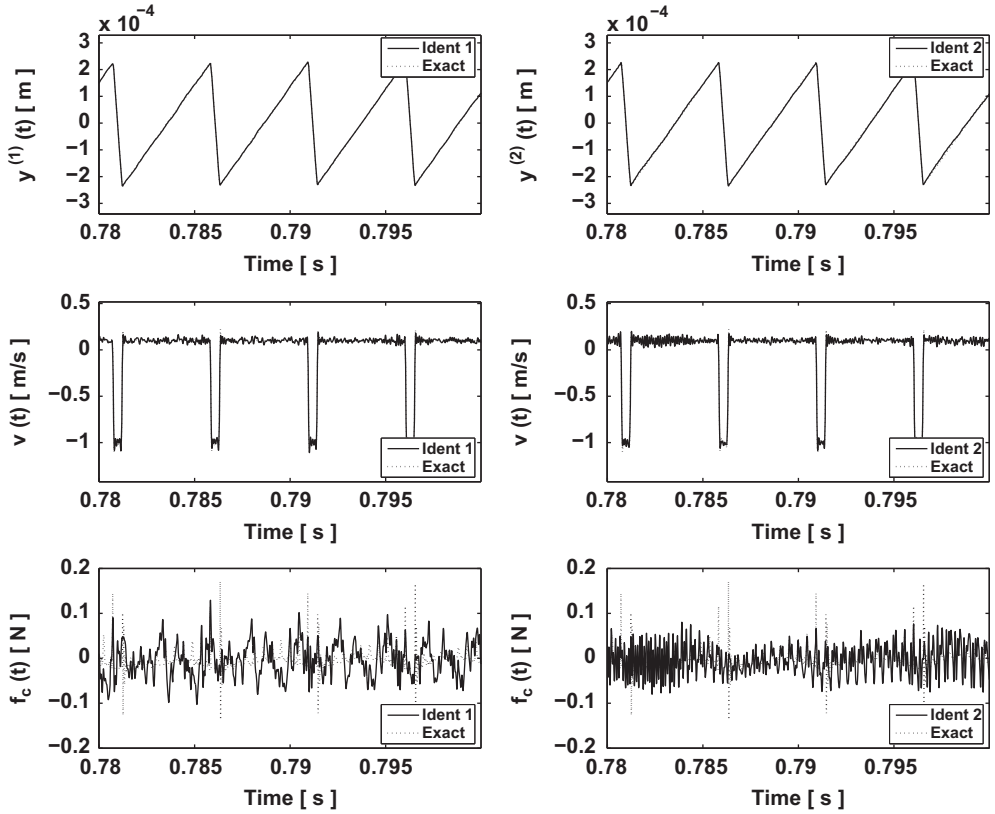


**Fig. 8.** Computed (dot) and identified (solid) time-histories of the displacement (up), velocity (middle) and frictional force (above) at the bowing contact point, obtained from the support reactions at $x=0$ (left) and $x=L$ (right), when noise is added to the support signals and no regularization procedure is applied. The level of noise is 8% of the standard deviation of the support reactions. $N=50$ modes.

where $\varepsilon$ is a regularization parameter which acts as a lower boundary on $H^{(r)}$ beyond which filtering of the inverse problem is enabled. Eq. (15) immediately brings up the question of what should be the value of the regularization parameter $\varepsilon$. Actually, selecting an appropriate $\varepsilon$ is essential to filter out the noise significantly, while still recovering important features of the solution. Several methods have been proposed to select a correct $\varepsilon$, amongst others the classical L-curve method and Generalized Cross Validation [25,26]. The L-curve diagram, where the norm of the regularized solution is plotted as a function of the residual norm in a log–log scale, works well in practice. However, its implementation could be difficult and sometimes the characterization of the corner of the curve—which is a good choice of the regularization parameter—fails. In this study, the selection of the regularization parameter is achieved by using the minimal product criterion [14]. The method aims to minimize the product between the norm of a convenient measure and the norm of the corresponding residual. Its underlying concept is consistent with the L-curve approach and its implementation has the advantage to be quite straightforward.

In our identifications, we observed that the classic L-curve diagram, as described before, does not result in a curve having a L-shaped appearance. However, the L-curve method could also deal with other measures of the solution in its general formulation [24,27]. By plotting the first derivative of the force in the vertical axis, a classic L-curve occurs, as attested in Fig. 9. The regularization constrains the influence of noise in the high frequencies and also at anti-resonance. As a consequence, we expect to recover reasonably the relevant low and high frequency contents in the solution. Fig. 9 also illustrates the product curve by which the selection of the regularization parameter is computed. The ordinate is the norm of the first derivative of the identified force, while the abscissa is the regularization parameter plotted with a log–log scale. The selected $\varepsilon$ value corresponds to the minimum of the product curve, and one can see that the method picks effectively a value placed in the corner region of the corresponding L-curve.

The benefit of the regularization is evident by comparing the identification results shown in Figs. 8 and 10 obtained when noisy support reaction signals are considered. For the results in Fig. 10, the regularization was used while in Fig. 8 the inversion was computed without precautions from Eqs. (10)–(13). The results for the identified forces are clear in showing the noise attenuation when regularization is performed. The selected regularization parameter values, computed by the minimum product method, are $\varepsilon_1=0.82$ and $\varepsilon_2=1.02$ for the identifications from the support reaction at $x=0$ and x=$L$, respectively. In Fig. 10, one notes that the larger $\varepsilon$, the more filtered are the identifications. Moreover, it is observed that the high frequency information at the beginning and end of the slipping stage is missing in the two identified forces, because regularization has the effect of a filter. To recover such details, improvement of the method could be done by incorporating some physical constraints, but for the present system, no such a priori information can be easily supplied.

To illustrate the accuracy of the technique, a measure of the difference between the identified and true friction force waveforms is proposed in terms of the correlation coefficients. The correlation coefficients between two signals $x$ and $y$ is defined in terms of their covariance $\sigma_{xy}$ and standard deviations $\sigma_x$ and $\sigma_y$, respectively, as

$$\mathcal{R}_{xy}=\frac{\sigma_{xy}}{\sigma_x\sigma_y}. \tag{16}$$

For uncorrelated signals, the coefficient is zero while equivalent signals result in correlation coefficient of 1. The accuracy of the

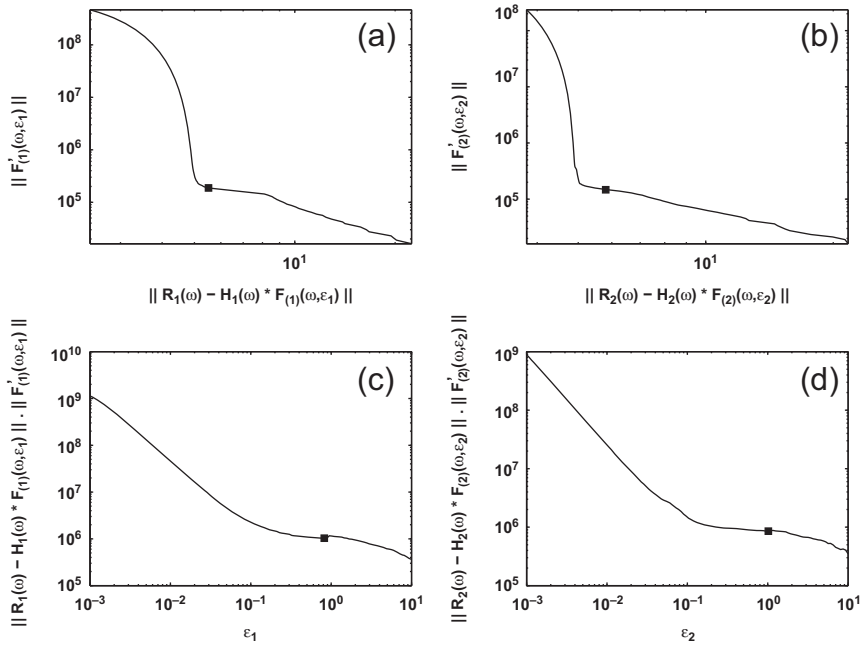


**Fig. 9.** Typical L-curves (up) and corresponding product curves (above) obtained from the support reactions at $x=0$ (left) and $x=L$ (right) when noise is added to the support end signals. The level of noise is 8% of the standard deviation of the support reactions. (a) and (b) The L-curve plots the norm of the force derivative versus the norm of the residue, as a function of the regularization parameter $\varepsilon$. (c) and (d) The product curve plots the product of the norm of the force derivative and of the residue as a function of $\varepsilon$. The selected regularization parameter (■) determined by the minimum product method (i.e. when the product reaches a local minimum) is placed in the corner region of the L-curve. Left: $\varepsilon_1 = 0.82$. Right: $\varepsilon_2 = 1.02$.

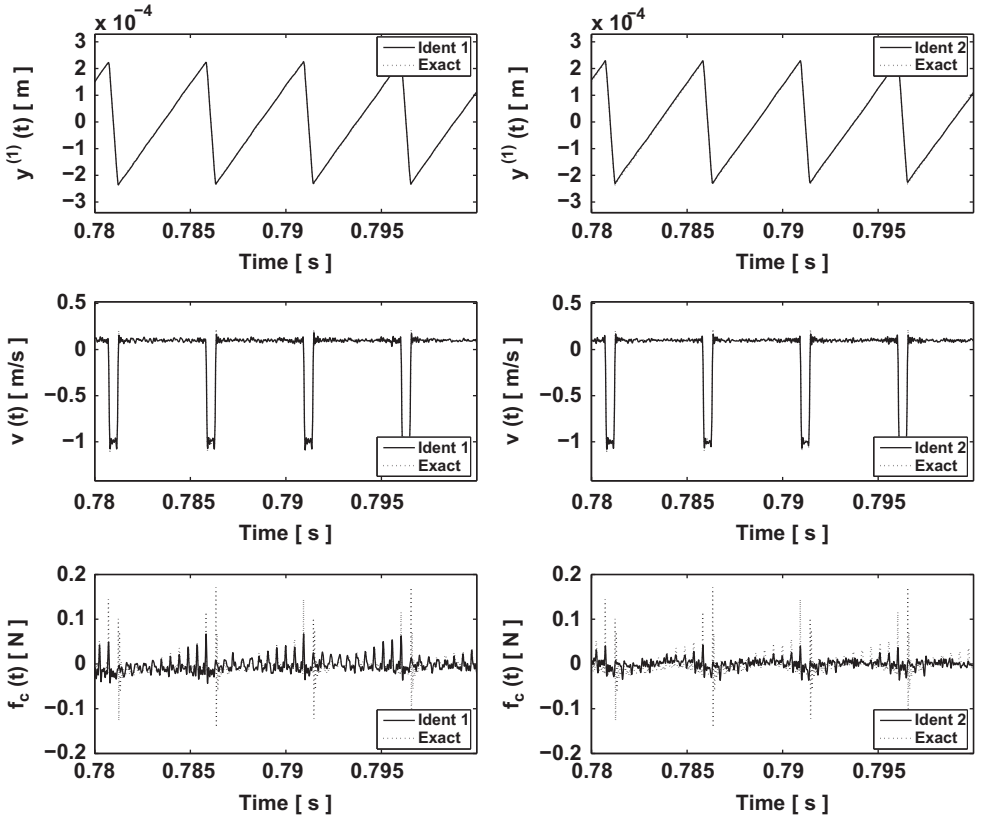


**Fig. 10.** Computed (dot) and identified (solid) time-histories of the displacement (up), velocity (middle) and frictional force (above) at the bowing contact point, obtained from the support reactions at $x=0$ (left) and $x=L$ (right), when noise is added to the support end signals and regularization is performed. The level of noise is 8% of the standard deviation of the support reactions. $N=50$ modes. The regularization parameter values used for the identifications are $\varepsilon_1 = 0.82$ (right) and $\varepsilon_2 = 1.02$ (left). Note the filtering effect performed by the regularization.

**Table 1**
Difference between the identified $f_c^{(i)}$ $(i=1,2)$ and the simulated $f_c$ friction forces in terms of the correlation coefficients $\mathcal{R}$, for different noise levels. Two periods of the steady state regime are used for the calculation. The corresponding regularization parameters $\varepsilon_i$ obtained by the minimum product method are also given.

| Noise level (%) | $\mathcal{R}_{f_c^{(1)} f_c}$ | $\varepsilon_1$ | $\mathcal{R}_{f_c^{(2)} f_c}$ | $\varepsilon_2$ |
|---|---|---|---|---|
| 0 | 0.81 | 0.01 | 0.95 | 0.002 |
| 1 | 0.71 | 0.07 | 0.67 | 0.08 |
| 2 | 0.65 | 0.17 | 0.63 | 0.08 |
| 3 | 0.60 | 0.26 | 0.50 | 0.30 |
| 4 | 0.62 | 0.40 | 0.48 | 0.37 |
| 5 | 0.60 | 0.40 | 0.48 | 0.61 |
| 8 | 0.60 | 0.82 | 0.48 | 1.01 |
| 10 | 0.59 | 0.88 | 0.45 | 1.01 |

identifications for different noise levels is presented in Table 1. As expected, the differences between the identified and true friction forces increase with the noise level as well as the regularization parameters. Our identifications also show that the $\varepsilon$ computed by the minimum product method departs from the corner of the L-curve as the noise level increases while the corner still remains. This indicates a lack in the selection technique and suggests that more efforts have to be done for such cases, probably by balancing other measure of the solution. Another interesting aspect to note is that the quality of the identification obtained from the support reaction signal closer to the bowing point is usually better.

## 6. An approach for dealing with uncertainty in the modal frequencies

As pointed earlier, the choice of a modal representation for the string imposes to have good knowledge of all the modal parameters needed to construct the system transfer functions. In a real situation, the modal parameters are inferred from modal computations or extracted from experimental data, by modal identification techniques [28]. They usually provide accurate estimates, but some errors always occur from either a faulty modal data acquisition procedure or a bias in the numerical algorithm. These arguments motivate to assess the problem of modal uncertainty, which is an essential issue of identification techniques, although seldom considered in the literature.

A peculiar aspect in our results is that identifications are somewhat tolerant to errors in modal damping. Actually, Fig. 11 shows results for the identified displacement, velocity and force at the contact point when an uncertainty of 50% is added to the damping values, superimposed to the true signals. An interesting aspect in Fig. 11 is that identifications remain globally in accordance to the true results. Physically, it suggests that for the bowed string, the internal damping and reflection losses at the string supports—which are included in the modal damping values $\zeta_n$—play only a modest role in the bowed-string dynamics. In other words, dissipation—which is essential for maintaining a stable oscillating regime—originates mainly from friction, for a bowed string. For our purpose, this is surely a convenient point. Actually, the optimization of the modal damping parameters is no longer required.

Contrary to modal damping, the problem of errors in the modal frequencies must be fixed, as stated earlier (see Fig. 4). Looking at Fig. 12, where the corresponding spectra of the identified forces in Fig. 4 are plotted, a careful examination of the spectra reveals that the effects of errors in the modal frequencies manifest as errors in the peaks amplitudes. To solve this problem, we then suggest that an effective solution could be to find the modal frequencies which reduce the amplitudes of these spurious peaks.

Based on this idea, our approach is to perform an optimization of the identified force spectra, mode by mode, by systematic search of the optimal modal frequencies. In addition to that, our approach is iterative in the sense that, when optimizing each successive modal frequency, we include the contribution of all the other modes within the frequency range of the optimized one. Therefore, several modal optimization loops enable a refinement of the optimal results.

Looking for a better estimate of each modal frequency $\omega_n^\star$, within a range of candidates $\omega_n^{test}$, we proceed as follows:

1. For a candidate frequency $\omega_n^{test}$, compute the system transfer function by superposition of all modes following Eq. (11).
2. Apply a pass-band filter centered at the frequency $\omega_n^\star$ to both the transfer function and the support reaction spectrum.
3. Identify the force from the filtered signals following Eq. (14) and compute the objective function defined as

$$\mathcal{C}(\omega_n^{test}) = \int_{\omega_n^\star-\Delta\omega_n}^{\omega_n^\star+\Delta\omega_n} |F_c(\omega_n^{test},\omega)|\, d\omega, \tag{17}$$

   where $F_c(\omega_n^{test},\omega)$ is the spectrum of the identified force.
4. Repeat steps 1–3 for each candidate $\omega_n^{test}$ and minimize Eq. (17).

Finally, by repeating the procedure for all the modes $n=1,2,\ldots,N$, a new set of optimized modal frequencies $\{\omega_n^\star\}$ is obtained. As stated before, the convergence can be somewhat improved by coupling this mode-by-mode optimization with an iterative procedure to incorporate the effects of the adjacent peaks. Actually, the optimization can be performed several times, from the new successive modal frequencies configurations $\{\omega_n^\star\}$. This has been done in the present identifications, for which 10 iterations are sufficient to converge. The search range of the candidates, as well as the integration boundaries $\Delta\omega_n$ (which determines the bandwidth of the pass-band filter) are a small percentage of the original $\omega_n^\star$ (respectively, $\pm 3\%$ and $\pm 4\%$).

Fig. 13 plots the objective functions for the first 12 modes, computed by testing 50 candidates for each mode. An uncertainty of 2% has been added to the modal frequencies initially and $N=50$ modes have been used for the modal basis. It is noteworthy that a single well-defined minimum occurs near the exact modal frequency, and that the optimization procedure converges to it as expected. Fig. 14 shows that for all the modes, the relative error remains small. However, one notes that the absolute error in the determination of the optimal frequencies globally increases with the mode index and becomes large for modes presenting a node at the contact point. It is a self-evident consequence of the modal approach, since no energy can be transmitted to these modes by the excitation. To overcome such inherent error, a fit of the optimized modal frequencies could provide good estimates for the modal frequencies of these unexcited modes (see Section 7).

Finally, Figs. 15–17 show, beyond the real signals at the contact point, the identifications of the string displacement and velocity, as well as the friction force, obtained after optimization of the modal frequencies. It can be seen that the method is capable of giving convincing identifications for all quantities, both during transient and steady state regimes. Both the displacement and the velocity of the string are in good agreement with the simulated signals. The identifications of the friction force are

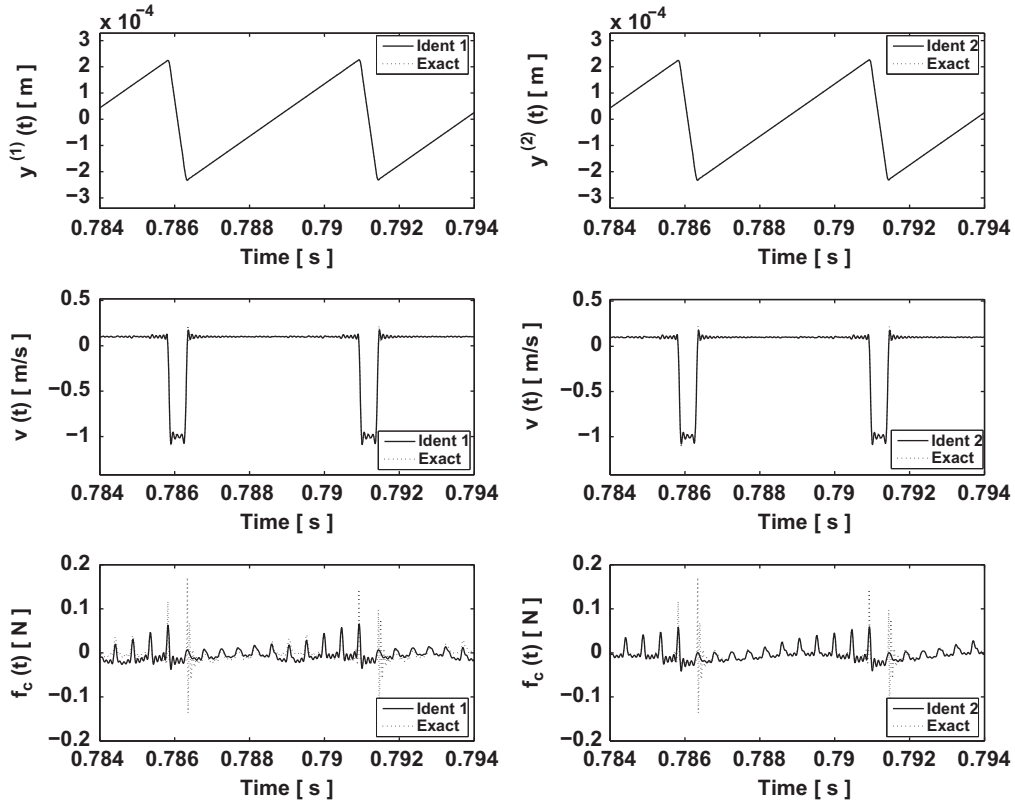


**Fig. 11.** Computed (dot) and identified (solid) time-histories of the displacement (up), velocity (middle) and frictional force (above) at the bow contact point, obtained from the support reactions at $x=0$ (left) and $x=L$ (right), when less-than-exact modal damping values are used. Uncertainty in the modal damping is 50%. $N=$ 50 modes.

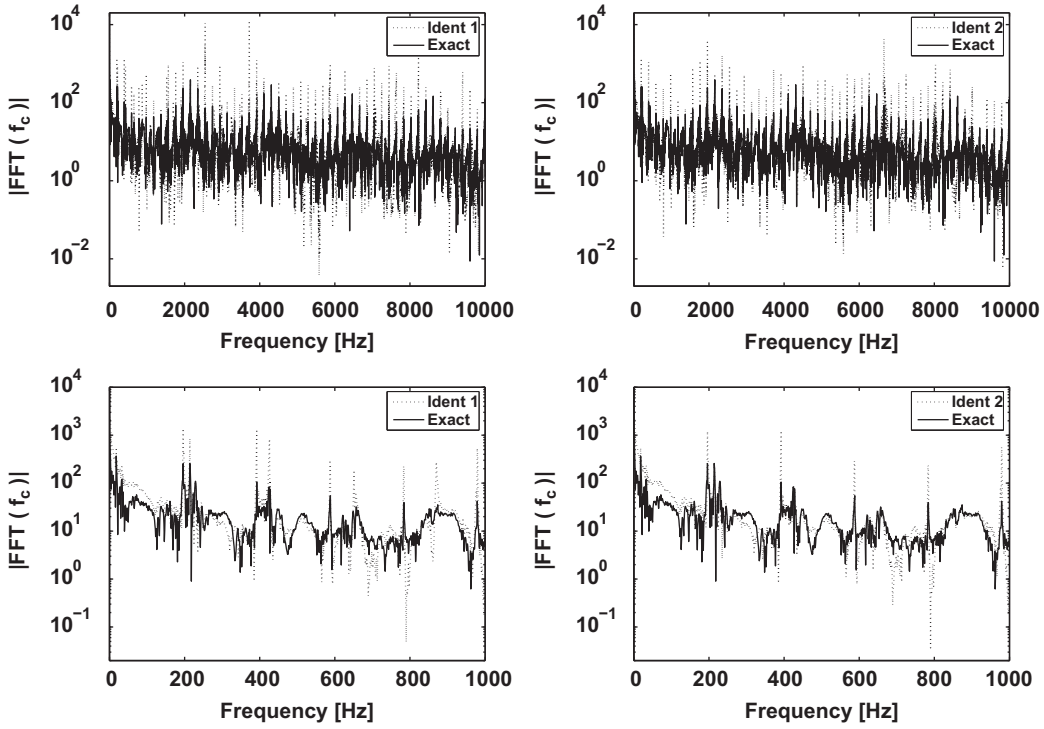


**Fig. 12.** Spectra of the computed (solid) and identified (dot) frictional forces obtained from the support reactions at $x=0$ (left) and $x=L$ (right), when less-than-exact modal frequencies are used. Uncertainty in the modal frequencies is 2%. $N=50$ modes. Note that errors in the modal frequencies manifest through the generation of spurious peaks in the identifications.

reasonable faithfull to the true result, globally. And as it can be noticed by comparing results in Figs. 4 and 17, the optimization improves undoubtedly the identifications. Results also show that the identification procedure seems reliable, because the reconstructions from one or the other support reaction are very similar.

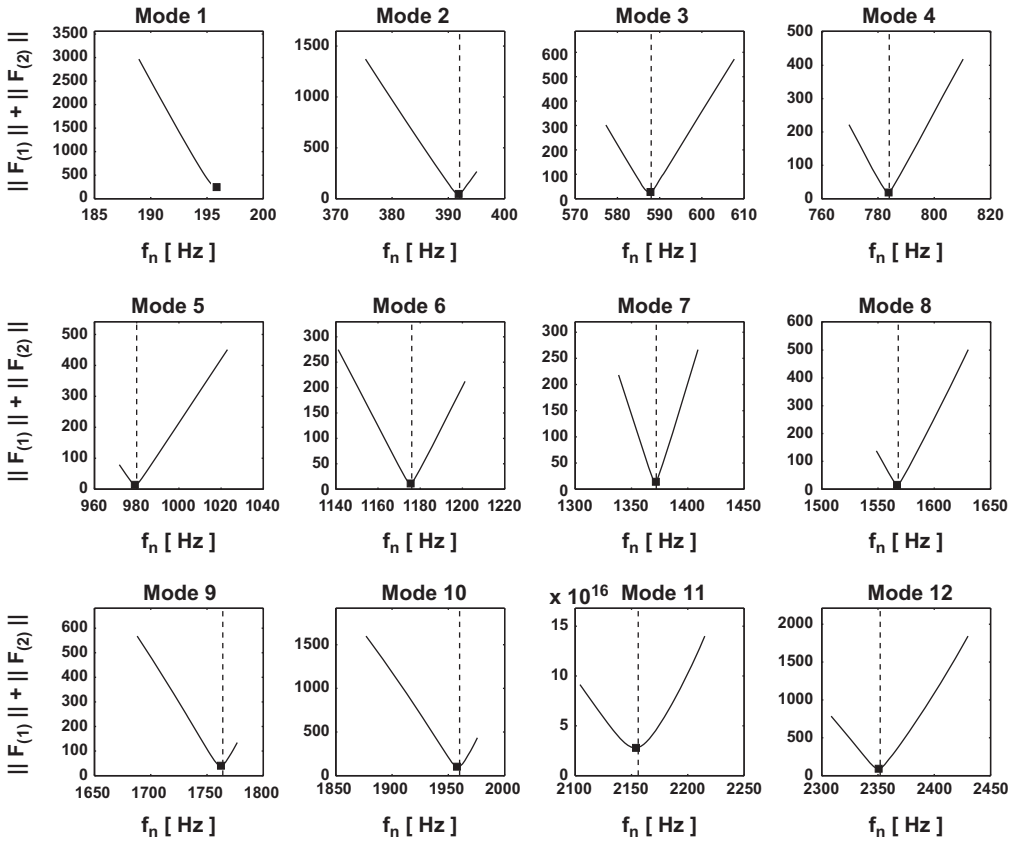


**Fig. 13.** Objective functions computed for the minimization of the identified force spectra as the modal frequencies candidate $\omega_n^*$ varies (only the first 12 modes ($n=1,\ldots,12$) are shown). The objective function is given by Eq. (17). Note that a net minimum occurs near the exact value (dotted line) of the modal frequency and that the optimization procedure converges to it (■).

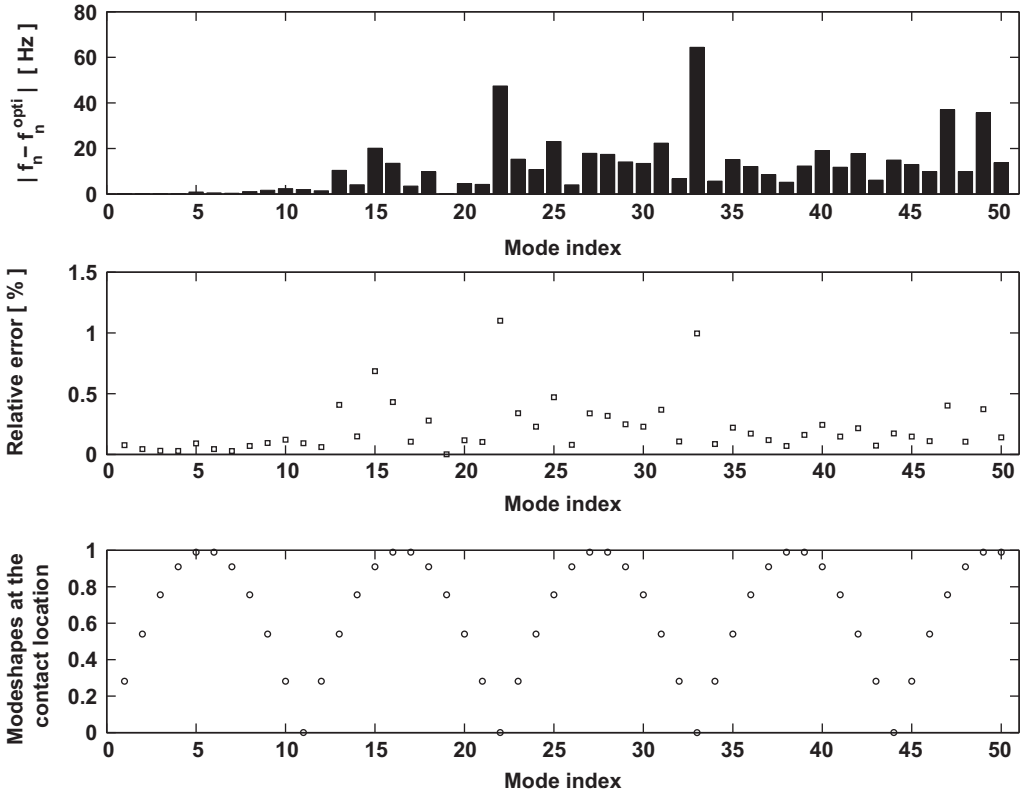


**Fig. 14.** Absolute (up) and relative errors (middle) in the optimized modal frequencies and values of the modeshapes at the contact point location (above), as a function of the mode index. Note that the absolute errors in the modal frequency are large when modes have a vibration node near the bow contact point.

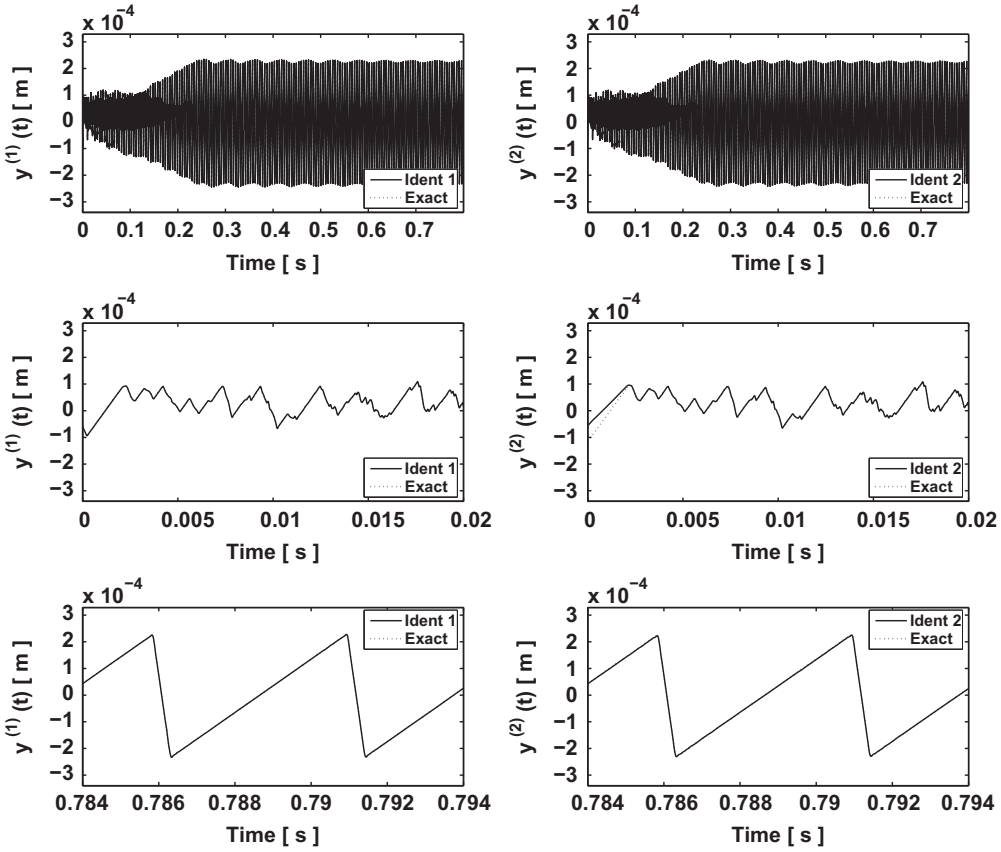


**Fig. 15.** Computed (dot) and identified (solid) time-histories of the string displacement at the bow contact point, obtained from the support reactions at $x=0$ (left) and $x=L$ (right), after optimization of the modal frequencies. Uncertainty in the modal frequencies is 2%. $N=50$ modes. Global time history trace (up) and details during initial transient (middle) and steady state regime (above).

## 7. Preliminary experimental identifications

Although the modal-based identification method provides exploitable and reliable results from simulated data, the complete technique will be convincing only after experimental identification is performed. Therefore, we present hereby the results from a preliminary set of experiments.

### 7.1. Experimental set-up

The string is driven by a very basic bowing device as seen in Fig. 18. The transverse motion of the bow is ensured through use of a couple of parallel flexible beams which guides the bow fixture. The normal force of the bow acting on the string and the location of the bowing point can be adjusted. Two piezoelectric force sensors B&K 8200, which respond to the transverse force exerted by the string at both ends, provide the signals $R_1(t)$ and $R_2(t)$ needed for the reconstructions. The velocity of the bow can be deduced from the accelerometer B&K 4375 attached to the bow. The signals were digitalized at a rate of 51 200 Hz through a Siglab model 20–42 acquisition board. An experimental run consists on releasing the bow, which performs several bowings in opposite directions until it stops. Measurements were done on a violin G string excited by the wood of the bow, usually known by the italian term *col legno*. This enables a well-localized contact point, which suits our preliminary experiments. The bow stick was also straightened by increasing the hair tension. The string is wound, with length 0.33 m, and a fundamental frequency of 196 Hz, the bowing contact point being at $x_c = 0.0285$ m ($\pm 1$ mm). Fig. 19 shows the measured dynamical reactions at end supports for one stroke. The bow velocity is zero at the beginning, then passes a maximum at the middle of the run and returns to zero at the end. The waveforms of the measured transverse forces display the classic sawtooth time-dependence, usually encountered, with the superimposed secondary waves which develop between the bow and the nearest end support. One can also notice the short transient before reaching the steady state regime.

An experimental modal identification of the string has been performed, from pluck tests, and extraction of the string modal parameters $\omega_n^\star$ and $\zeta_n$ was achieved by implementing an ERA algorithm [29]. The modal mass $m_n$ and modeshapes $\varphi_n$ are computed from the classic theoretical expressions found in Ref. [30], for instance. Eleven modes were well identified experimentally. As expected, because of the string stiffness, the modal frequencies are not perfectly harmonic. The identified damping values increase with the modal index, and are as small as 0.02% for the lowest modes.

As pointed earlier, the choice of the modal basis truncation order has to be asserted with care, based on physical reasoning. With respect of the present system, it is known that a large number of modes contributes to the self-excited motion of the bowed string [4,31]. Furthermore, the order of truncation is linked to the spread of the excitation which gives the spatial resolution. Actually, point-force identifications become incorrect when the modeshape inter-nodal lengths are comparable with the width of the bow. In our example, the contact width region is approximately 2 mm. Then, assuming a larger value corresponding to three times the contact width, the order of truncation is chosen as $N=55$.

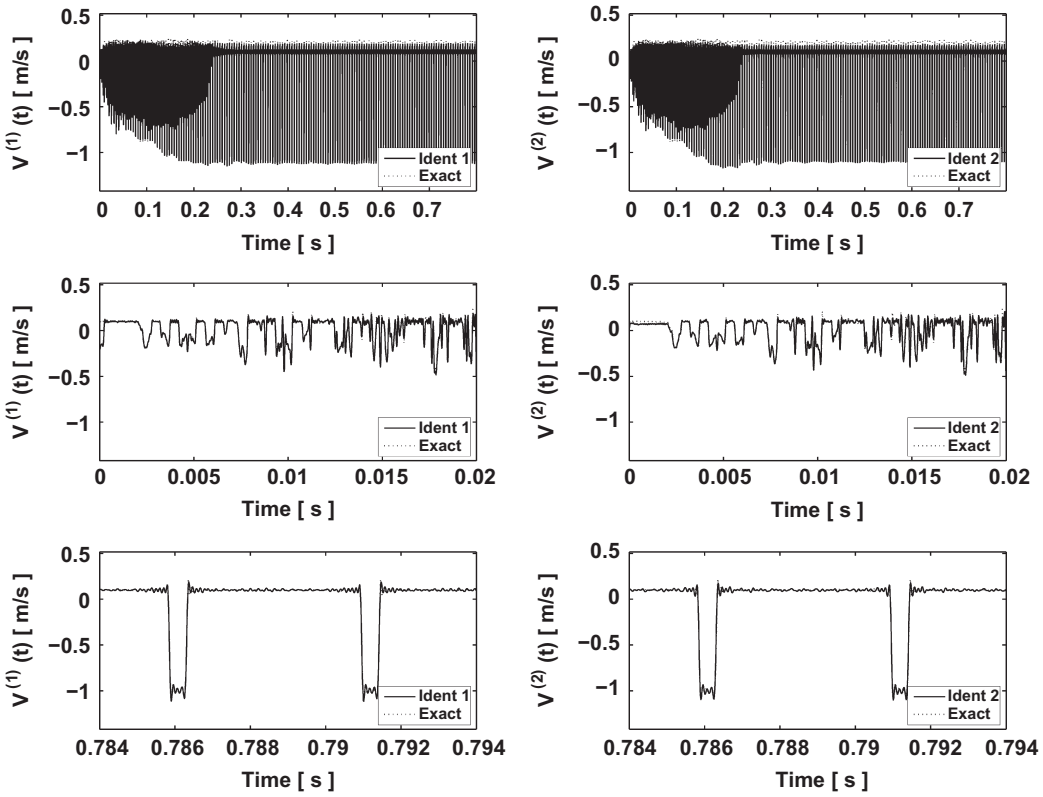


**Fig. 16.** Computed (dot) and identified (solid) time-histories of the string velocity at the bow contact point, obtained from the support reactions at $x=0$ (left) and $x=L$ (right), after optimization of the modal frequencies. Uncertainty in the modal frequencies is 2%. $N=50$ modes. Global time history trace (up) and details during initial transient (middle) and steady state regime (above).

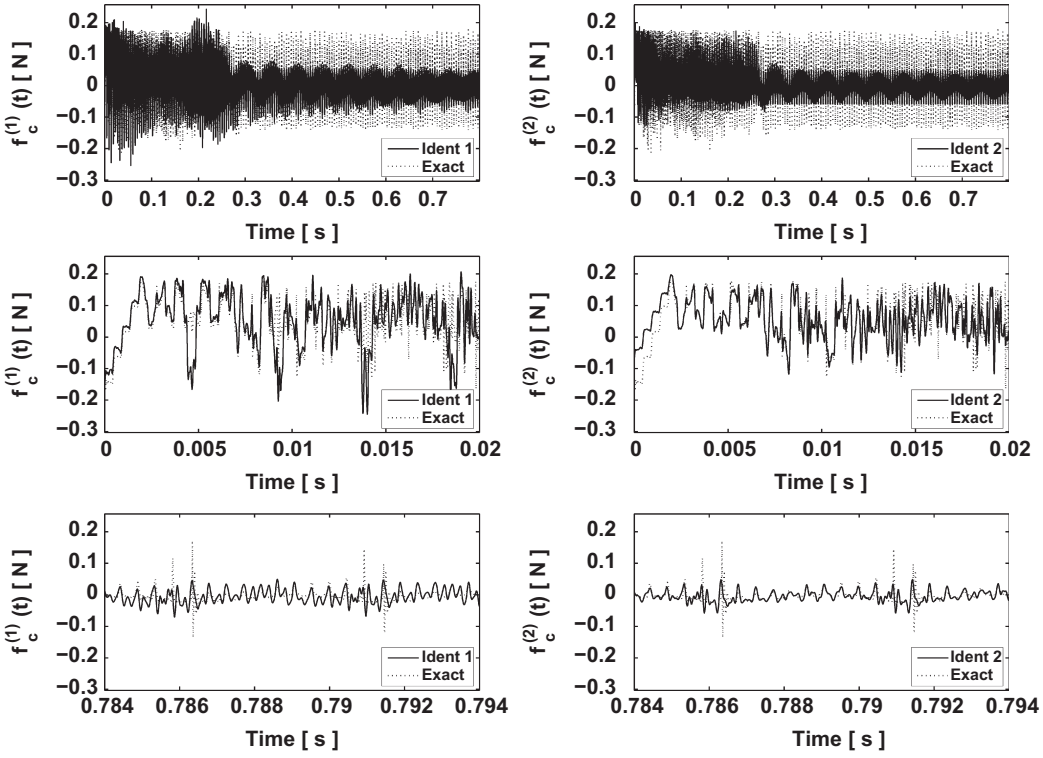


**Fig. 17.** Computed (dot) and identified (solid) time-histories of the frictional force at the bow contact point, obtained from the support reactions at $x=0$ (left) and $x=L$ (right), after optimization of the modal frequencies. Uncertainty in the modal frequencies is 2%. $N=50$ modes. Global time history trace (up) and details during initial transient (middle) and steady state regime (above).

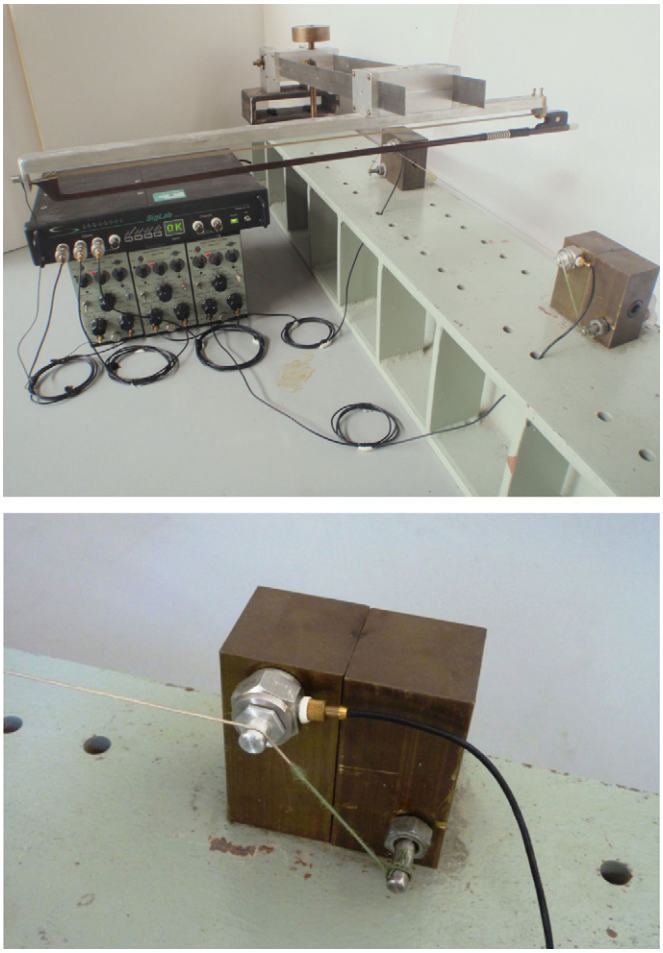

**Fig. 18.** Upper picture: experimental set-up with the bowing device and the data acquisition system. Lower picture: the string and one support force sensor.

To increase the size of the modal basis identified from the pluck tests (only 11 modes were accurately identified), a fitting procedure is now combined to the optimization scheme described in Section 6. Bearing in mind the results in Fig. 14, one understands that a fit of the optimized frequencies can suffer from the poor estimation of the modes with a vibration node at the bowing point. For instance, a fit involving 22 modes will not provide a good fit. To avoid such situation, we begin with the optimization of the first five identified modal frequencies and then use these estimates to get a reliable fit of the experimental system modal frequencies using [30]:

$$\omega_n = n\omega_1\sqrt{1+Bn^2} \quad \text{for } n \geq 2, \tag{18}$$

where $\omega_1$ is the optimized fundamental frequency of the string and $B$ is the string inharmonicity coefficient. A value of $B = 1.54 \times 10^{-4}$ is computed in the least square sense (note that the identification is nonlinear) and then, Eq. (18) is used to infer the required 55 modal frequencies. However, for a better match with the experimental system, more accurate estimates of these frequencies can be obtained by optimizing the identified spectra and using the 55 fitted modal frequencies as the initial set (see Section 6). As shown in Fig. 20, a well-defined minimum occurs for the objective function given by Eq. (17). It is interesting to note that this feature is observed for all modes which gives some confidence in the use of the optimization approach from measured data. However, since the errors in the modal frequencies are large for modes presenting a node at the contact point, we prefer to use for the less-excited modes values inferred from an interpolation of the 55 optimized modal frequencies according to Eq. (18) for which the string inharmonicity coefficient is found to be $B = 1.39 \times 10^{-4}$. In the presented identifications, it concerns modes 11, 12, 22, 34 and 45. For the other modes, the modal frequencies stemming from the optimization of the identified force spectra have been used.

For the modal damping, the 11 measured values for the experimental string are first fitted choosing arbitrarily a

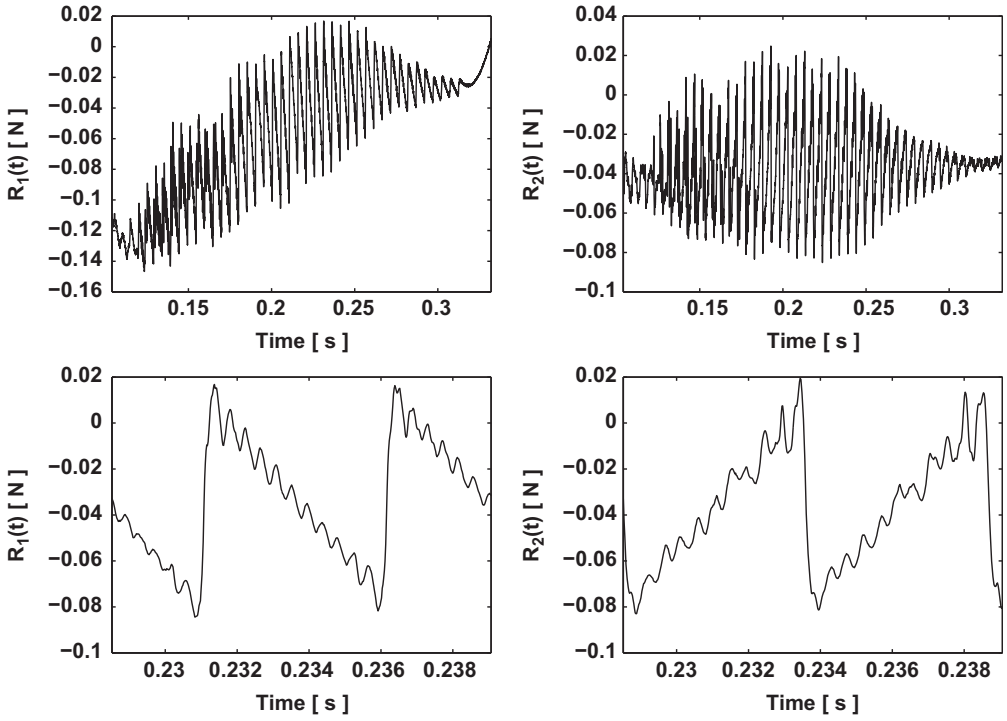


**Fig. 19.** Measured dynamical support reactions at $x = 0$ (left) and $x = L$ (right) from the experimental system for one stroke. Time-histories: global time history trace (up) and detail during a periodic motion of the string (above).

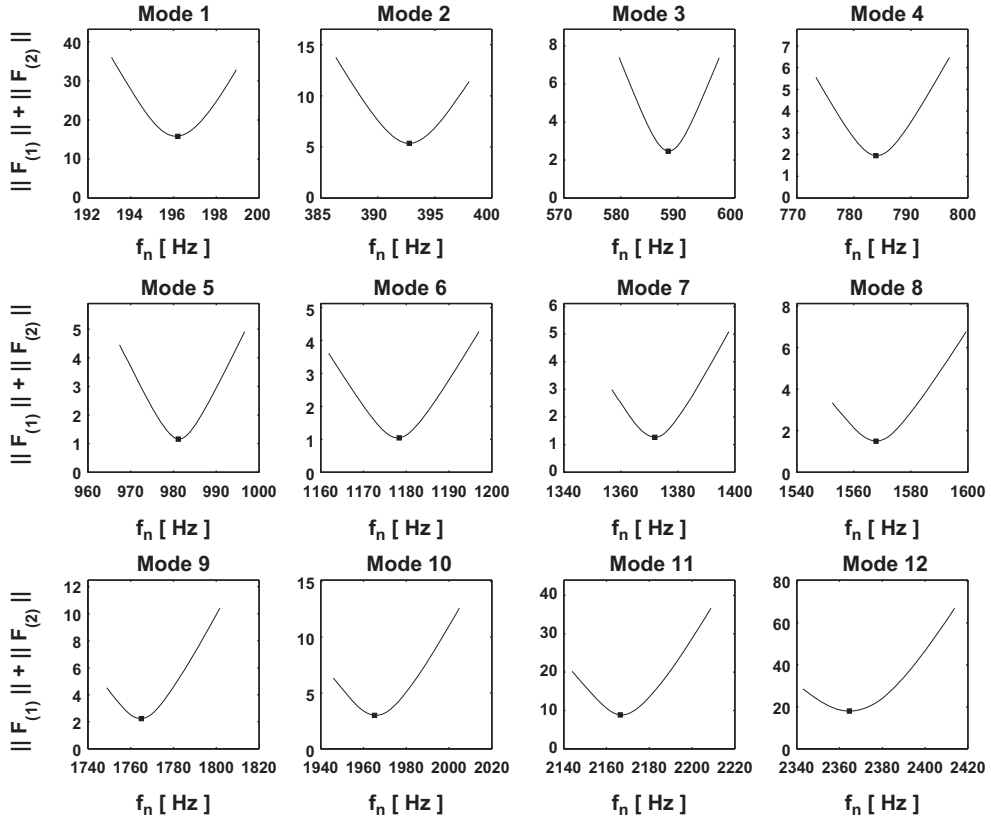


**Fig. 20.** Objective functions computed for the minimization of the experimentally identified force spectra as the modal frequencies candidate $\omega_n^*$ varies (only the first 12 modes ($n=1,\ldots,12$) are shown). The objective function is given by Eq. (17). Optimal frequencies chosen for the identifications are noted by ■. Note that they correspond to a net local minimum of the objective function.

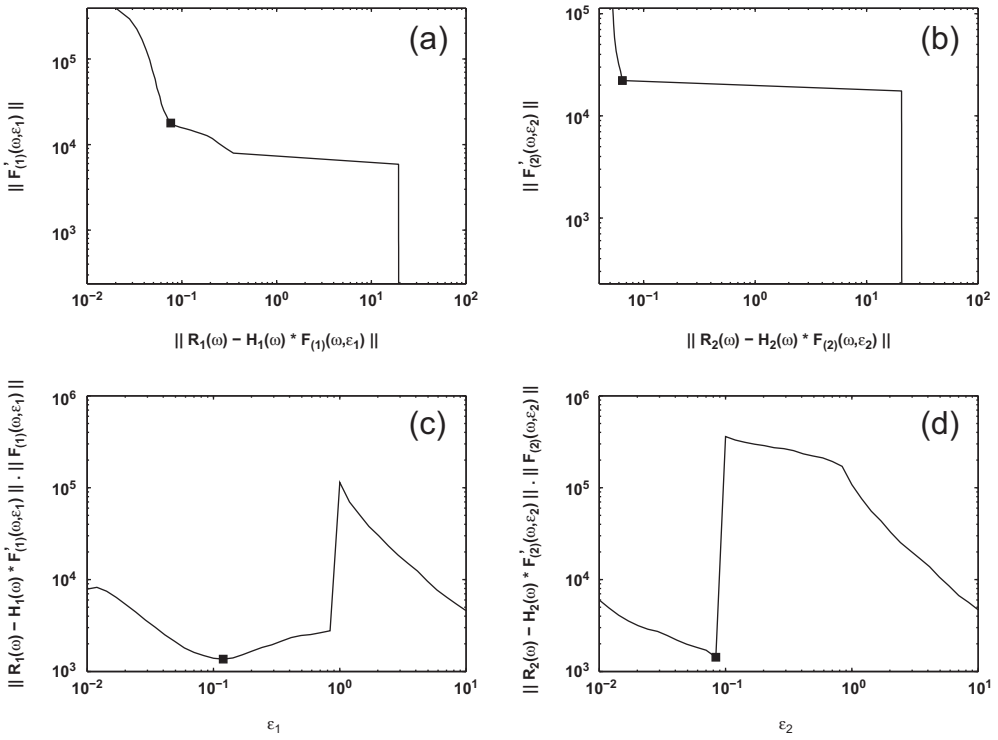


**Fig. 21.** (a) and (b) L-curves obtained from the measured support reactions at $x=0$ (left) and $x=L$ (right). (c) and (d) Corresponding product curves. Left: $\varepsilon_1=0.12$. Right: $\varepsilon_2=0.08$. Note that the selected regularization parameters determined by the minimum product method are near the corner of the corresponding L-curves.

polynomial of degree 2 and the damping values for the 55 modes are extrapolated using the corresponding polynomial.

Fig. 21 shows the L-curves and corresponding product curves obtained by applying the regularization technique described in Section 5 and using the dynamical reactions measured at $x=0$ and $x=L$. The regularization parameters determined by the minimum product method are found to be $\varepsilon_1 = 0.12$ and $\varepsilon_2 = 0.08$, respectively, and it is reassuring to see that these values are near the corner of the corresponding L-curves.

### 7.2. Identifications of the displacement, velocity and frictional force

Fig. 22 shows the identified string displacement, velocity and frictional force at the contact point from the two string support reactions during a nearly periodic motion of the string. A modal basis of $N=55$ modes has been used for identifications and the contact point location has been adjusted to minimize the difference between the two identified force waveforms ($x_c = 0.0285$ m). It appears that the string has developed a Helmholtz regime with the resulting stick–slip vibration displayed by the displacement and velocity signals.

As attested by the comparison of pair identifications, which is here the only measure to assess the correct behaviour of the method, the technique seems to be consistent. It is satisfying to see that the two versions of the reconstructed signals are very similar, differing only in local details, for both the string dynamic responses and the friction force. Besides, by computing the bow velocity from the accelerometer attached to the bow, one can verify that the bow velocity during adherence is of the order $0.01\,\mathrm{m\,s^{-1}}$ as found in the velocity plot in Fig. 22. Note that the bow velocity is then ten times lower than the value used in the simulations (see Fig. 2).

An interesting feature of the identified forces in Fig. 22 is the quasi-periodic and large fluctuations measured during the (assumed) adherence stage of the string motion. Actually, the comparison between the identified and simulated forces (see Fig. 2) shows that these oscillations are more strongly pronounced in the experimentally identified signals. If we assume that similarities of the left and right identifications warrant the identification quality, two physical reasons could explain this difference. First, it could be related to the difference in the bow velocity between the computation and experiment. However, it is most probably due to the presence of secondary torsional waves which developed between the bow and the nearest end support. Actually, the model used in the simulations has been established by neglecting the torsional motion of the string, whereas it is expected that torsional waves couple with transverse waves in the experiments, because they are both strongly excited at the contact point [31]. In Fig. 22, the string's torsional motion is highlighted by the fluctuations in the string velocity during adherence. It should be noted that our measurements are obtained when bowing the string with the wood stick, which has a much greater axial stiffness than the bow hair, thus preventing any significant vibrations of the string contact point during adherence. Now, an interesting fact is that the effects of torsional waves are likely reflected somehow in our identification procedure. Actually, it is important to emphasise that if the eigenfrequencies and damping factors differ for transverse and torsional vibrations, their modeshapes are similar. Part of the torsional energy can thus be accounted in the product $\varphi_n(x_c)\varphi_n(x_c)$ in Eq. (11) even if the transfer function $H^{(r)}$ used in the identification procedure describes only the propagation of the transverse waves. Therefore, one may tentatively conclude that the torsion modes are responsible for the large observed fluctuations in the identified force. Much more is to be learned from the identification results, which will be reported at a later stage of this investigation.

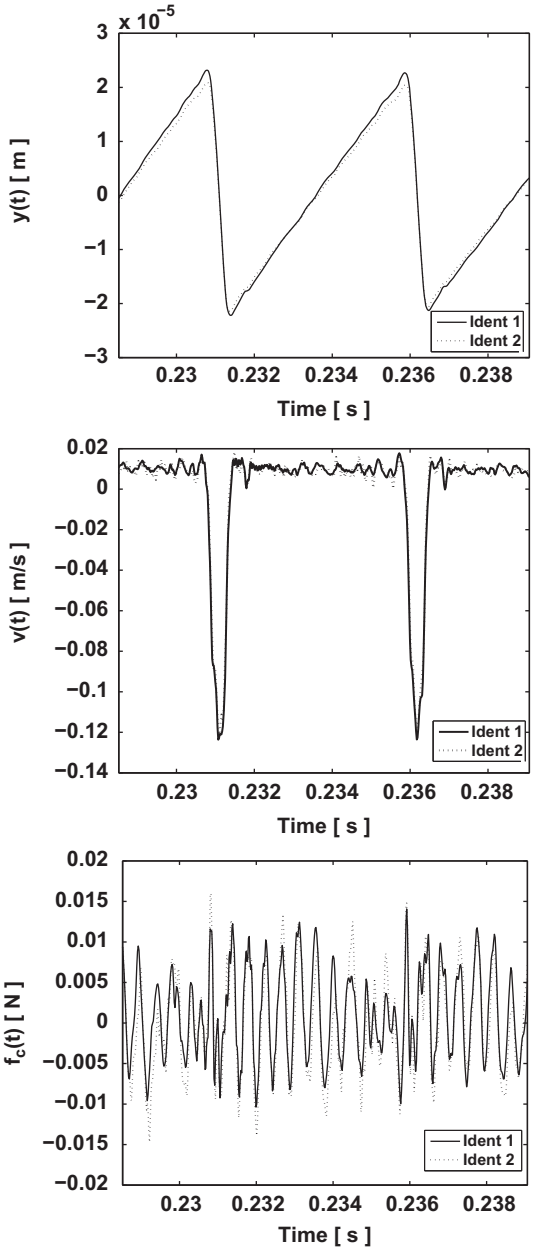


**Fig. 22.** Experimentally identified displacements (up), velocities (middle) and friction forces (above) at the bowed contact point. Two versions are shown, obtained by using separately the measured forces from the end supports at $x=0$ (solid) and $x=L$ (dot), respectively. Note that the two identifications give near-similar results for the displacement and velocity, and reasonably similar identifications for the friction force.

## 8. Conclusions

A method has been presented for the identification of the frictional nonlinear interaction force and string dynamics at the contact point for a bowed string. The identification procedure combines the use of regularization and optimization techniques to overcome difficulties due to polluting noise and modeling errors respectively.

In contrast to the previous efforts in this field, the present method uses a modal approach, which allows to deal easily with

the effects of wave reflections and damping at the string support ends. As a significant contribution, a technique to address the problem of modal uncertainty is presented. Optimization of the modal frequencies is achieved in the frequency domain, mode by mode, by systematic search, combined with an iterative procedure to include the contribution of all the modes within the frequency range of the optimized one. Results show that the technique improves significantly the identifications when small errors in the modal frequencies exist. The regularization of the problem has been achieved in the frequency domain, by forcing to zero the frequency terms in the inverse solution corresponding to small values of the transfer function.

The presented results give a good idea of the overall accuracy of the identification process, by comparison of our identifications with original simulated data stemming from nonlinear computations of the bowed string. The method provides reasonably convincing identifications of the string displacement, velocity and of the interaction force between the bow and the string. Finally, the technique was applied to experimental data, obtained by using a basic bowing device and driving the string with the stick of the bow. The agreement between the two versions of the frictional force is satisfactory and identification results are consistent. Extensive systematic experiments will now be performed, in order to better understand the different aspects of a real string bow excitation.

## References


[1] McIntyre ME, Schumacher RT, Woodhouse J. On the oscillations of musical instruments. J Acoust Soc Am 1983;74(5):1325–45.

[2] Woodhouse J. Self-sustained musical oscillators. In: Hirschberg A, Kergomard J, Weinreich G, editors. Mechanics of musical instruments. New-York, USA: Springer-Verlag; 1995. [chapter 5].

[3] Inácio O. A modal method for the simulation of nonlinear dynamical systems with application to bowed instruments. PhD thesis, University of Southampton; 2009.

[4] Gough C. Musical acoustics. In: Rossing TD, editor. Handbook of acoustics. New-York, USA: Springer-Verlag; 2007. p. 554–600.

[5] Smith JH, Woodhouse J. The tribology of Rosin. J Mech Phys Solids 2000;48:1633–81.

[6] Woodhouse J, Galluzo P. The bowed string as we know it today. Acustica 2004;90:579–89.

[7] Schumacher RT. Studies in bowing-point friction in bowed strings. J Acoust Soc Am 1998;103:2915.

[8] Woodhouse J, Schumacher R, Garoff S. Reconstruction of bowing point friction force in a bowed string. J Acoust Soc Am 2000:357–68.

[9] Antunes J, Paulino M, Piteau P. Remote identification of impact forces on loosely supported tubes: part 2—complex-vibro impact motions. J Sound Vib 1998;215:1043–64.

[10] Paulino M, Antunes J, Izquierdo P. Remote identification of impact forces on loosely supported tubes: analysis of multi-supported systems. ASME J Pressure Vessel Technol, Vib 1999;121:61–70.

[11] De Araujo M, Antunes J, Piteau P. Remote identification of impact forces on loosely supported tubes: part 1—basic theory and experiments. J Sound Vib 1998;215:1015–41.

[12] Delaune X, Antunes J, Debut V, Piteau P, Borsoi L. Modal techniques for remote identification of non-linear reactions at gap-supported tubes under turbulent excitation, PVP 2009 Prague, ASME J Pressure Vessel Technol, in press.

[13] Debut V, Bersac C, Antunes J. Identification of the dynamical bow/string friction interaction force from vibratory measurements using inverse methods. In: Proceedings of the ICSV 16. Krakow, 2009.

[14] Lian J, He B. A minimal product method and its application to cortical imaging. Brain Topogr 2001;13(3):209–17.

[15] Antunes J, Tafasca M, Henrique L. Simulation of the bowed-string dynamics: part 1—a nonlinear modal approach. In: Proceedings of the fifth french acoustics congress, 2000.

[16] Inácio O, Henrique L, Antunes J. Simulation of oscillation regimes of bowed bars: a nonlinear modal approach. Nonlinear Sci Numer Simulation 2006;8:77–95.

[17] Antunes J, Inácio O, Henrique L. Overview of nonlinear effects in impacted and self-excited musical instruments. In: Proceedings of the euromech colloquium 483, geometrically non-linear vibrations of structures, 2007.

[18] Inácio O, Antunes J, Wright M. Computational modelling of string-body interaction for the violin family and simulation of wolf notes. J Sound Vib 2007;310:260–86.

[19] Debut V. Deux études d'un instrument de musique de type clarinette: analyse des fréquences propres du résonateur et calcul des auto-oscillations par décomposition modale. PhD thesis, Université de la Méditerranée; 2004.

[20] Hart GC, Wong K. Structural dynamics for structural engineers. New York, USA: John Wiley & sons Inc.; 1999.

[21] Mammone RJ. Computational methods of signal recovery and recognition. New York, USA: John Wiley & Sons Inc.; 1992.

[22] Groetch CW. Inverse problems in the mathematical sciences. Wiesbaden, Germany: Vieweg; 1993.

[23] Randall RB. Frequency analysis, 3rd ed. Copenhagen: Brüel and Kjær; 1987.

[24] Aster R, Borchers B, Thurber C. Parameter estimation and inverse problems. Elsevier Academic Press; 2005. 〈http://www.citeulike.org/user/kanicka/article/4371754?citation_format=elsart-harv〉.

[25] Hansen P, O'Leary D. The use of the L-curve in the regularization of discrete ill-posed problems. SIAM J Sci Comput 1993;14(6):1487–503.

[26] Grech R, Cassar T, Muscat J, Camilleri K, Fabri S, Zervakis M, Xanthopoulos P, Sakkalis V, Vanrumste B. Review on solving the inverse problem in EGG source analysis. J NeuroEngineering Rehabil 2008;5(25):579–89.

[27] Busby HR, Trujillo DM. Optimal regularization of an inverse dynamics problem. Comput Struct 1997;63(2):243–8.

[28] Randall JA, David LB. Experimental modal analysis. In: Kobayashi AS, editor. Handbook on experimental mechanics, second revised ed. New-York, USA: VCH Publishers; 1993 [chapter 16].

[29] Juang J. Applied system identification. Upper Saddle River, NJ, USA: Prentice-Hall Inc.; 1994.

[30] Valette C, Cuesta C. Mécanique de la corde vibrante, Traité des nouvelles technologies, Hermès, Paris; 1993.

[31] Cremer L. The physics of the violin. Cambridge, USA: MIT Press; 1984.

[32] Askenfelt A. Measurement of bow motion and bow force in a violin playing. J Acoust Soc Am, 1986.